Mon. Not. R. Astron. Soc. **000**, 000–000 (0000) Printed 1 February 2008 (MN LATEX style file v1.4)

Determination of time delay from the gravitational lens B1422+231

A.R. Patnaik[1], D. Narasimha[2]
[1] *Max-Planck-Institut für Radioastronomie, Auf dem Hügel 69, D–53121 Bonn, FRG*
email: apatnaik@mpifr-bonn.mpg.de
[2] *Department of Astronomy and Astrophysics, TIFR, Homi Bhabha Road, Mumbai 400005, India.*
email: dna@astro.tifr.res.in

1 February 2008

ABSTRACT

We present the radio light curves of lensed images of the gravitational lens B1422+231. The observations have been carried out using the VLA at 8.4 and 15 GHz over a period of 197 days. We describe a method to estimate the time delay from the observed light curves. Using this method, our cross-correlation analysis shows that the time delay between images B and A is 1.5±1.4d, between A and C is 7.6±2.5d, between B and C is 8.2±2.0d. When applied to other lensed systems with measured time delays our new method gives comparable results.

Key words: gravitational lensing - quasar B1422+231 - time delay

1 INTRODUCTION

One of the most promising outcomes of the study of gravitational lensing is the potential to determine the Hubble constant, H_0, independent of the standard distance ladder (Refsdal 1964). The light travel times for the lensed images are not equal due to the geometrical path length difference caused by the gravitational potential of the lens. This results in a time delay between the lensed images that can be measured by monitoring the images over a period of time. Thus, given a measurement of time delay and a knowledge of the gravitational potential of the lens, one can estimate H_0. At present, the accuracy of H_0 values determined by this method is limited mainly by our knowledge of the mass distribution in the distant lensing galaxy.

So far, time-delay measurements are available for seven lensed systems. For the twin quasar 0957+561 the measured values at both radio and optical wavelengths are in agreement and have been confirmed by observing variability in the image B after it was recorded in the image A (Schild & Thomson 1997, Kundić et al. 1997b, Haarsma et al. 1999). While for this system a reliable measurement of the time delay has been achieved, translation into an estimate of the Hubble constant turns out to be not straightforward (Narasimha, 1999). For the systems PG 1115+080 (Schechter et al. 1997), B1608+656 (Fassnacht et al. 1999), PKS 1830-211 (Lovell et al. 1998), B1600+434 (Koopmans et al. 2000) the measured delays are less accurate, mainly because it is not easy to extract the intrinsic variability and determine its phase lag between the images. The system B0218+357 has good time delay measurements (Biggs et al. 1999) and the redshift combination of the lens and source are favourable for a possible determination of H_0, but the lens models continue to be ill-constrained. However, these systems together cover various combinations of the distance to the source and lens as well as the distance from the lens to the source; hence an estimate of the distance scale from time-delays in all these systems together would be an important step to determine the Hubble constant and the large scale geometry of the Universe.

The lens system B1422+231 is particularly interesting in this respect, as the redshift of the source, $z_S = 3.62$, (Patnaik et al. 1992) is very large compared to the redshift of the lens, $z_L = 0.33$, (Kundić et al. 1997a, Tonry 1998) and consequently, the time-delay is a more direct measure of the distance to the lens. B1422+231 is a quadruple system which has been observed at various wavebands (Patnaik et al. 1992; Lawrence et al. 1992; Remy et al. 1993; Yee & Ellingson 1994; Bechtold & Yee 1995; Akujor et al. 1996; Yee & Bechtold 1996; Impey et al. 1996). Several models have been presented to explain the lens system (Hogg & Blandford 1994, Narasimha & Patnaik, 1994, Kormann, Schneider & Bartlemann 1994, Mao & Schneider 1998). Detailed radio maps at sub-milliarcsecond resolution are available for the images (Patnaik et al. 1999) and the mapping of the resolved structures of the images can be used for construction of the lens models. Optical spectra of the images have been taken with high sensitivity (Impey et al. 1996) and the emis-

sion line profiles of strong lines like Lyα have been used by Narasimha & Srianand (1999) to constrain the lens models. Thus, it is clear that a measurement of the time-delay for this system will be useful for the calibration of the cosmic distance scale, even though the source is not highly variable.

2 OBSERVATIONS AND DATA ANALYSIS

The VLA monitoring campaign of the gravitational lens B1422+231 was carried out at two frequencies, 8.4 and 15 GHz between 1994 March 03 to September 16. We used two 50 MHz-wide IF bands at each frequency.

We used 3C286 (J1331+3030) to calibrate the flux density scale, OQ208 (J1407+2827) as the phase calibrator, and 3C287 (J1330+2509) as a control source since it is not expected to be a variable source. The other reason for selecting this source is that it is close to the declination of our target source to ensure proper calibration of gain as a function of elevation.

The observations were carried out for about 30 min on each day, the integration time for the target source was 5 min at each frequency and the rest of the time was used for observing the calibration and control sources. Accurate calibration is of vital importance in this kind of monitoring observations. The observations of the two calibrators ensure that any variations in them must be due to calibration errors and hence these variations can, at least partially, be removed from the light curve of the lensed images.

We chose two different frequencies in order to have confidence in the measurements of time delay as it is independent of frequency, though the variability of quasars does depend on the frequency in the sense that they tend to be more variable at higher frequencies. In the present case, we chose 8.4 and 15 GHz for the following reasons. In the A configuration of the VLA the resolutions are about 0.2 and 0.13 arcsec at 8.4 and 15 GHz respectively, which allows clean separation of the images. In the B configuration, however, the two brighter images, A and B, are blended together at 8.4 GHz since the resolution is three times poorer, while there is no such difficulty at 15 GHz. We can sample the light curve over the periods of A and B configurations of the VLA at 15 GHz but only during the A configuration at 8.4 GHz.

The data were calibrated and imaged using the AIPS software package of National Radio Astronomy Observatory. Assumed flux densities of 3C286 were 5.145 Jy and 5.124 Jy at the centre frequencies of the two IF bands which are 8.4149 GHz and 8.4649 GHz respectively, and 3.449 Jy and 3.457 Jy at 14.9649 GHz and 14.9149 GHz respectively. Since 3C286 is partially resolved at these frequencies, we followed the standard procedure in using the shortest baselines to set the scale of flux density.

We assumed that both OQ208 and 3C287 are unresolved sources and used them to determine the gain solutions. We then used the AIPS program GETJY to determine the flux densities of these two sources which are bootstrapped from 3C286. The source 3C287 is, in fact, partially resolved in the A-array (its flux density changes from 1.4 Jy at short spacings to 0.9 Jy at the longest spacing at 15GHz). We could have mapped the source to determine its flux density. However, the assumption that it is a point source affects its flux density measurement by only 0.5% (our method gets less flux density). Thus the assumption that 3C287 behaves as a point source is justified. Moreover, we avoid introducing errors as a result of the mapping process.

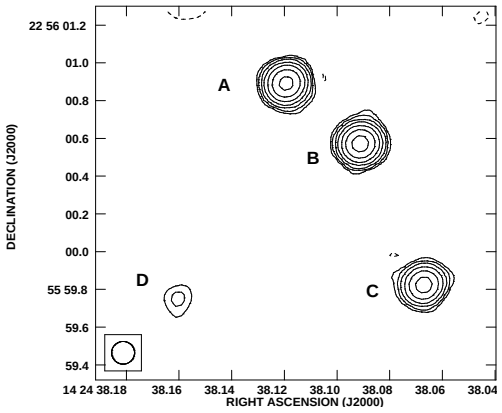

Figure 1. 15 GHz map of B1422+231. The map has been restored with a circular gaussian with FWHM of 0.2 arcsec, drawn at the bottom left hand corner. The contour levels are $-2, -1, 1, 2, 4, 8, 16, 32, 64$ mJy beam^{-1}. Negative contours are dashed. The rms noise in the map is 0.37 mJy beam^{-1}. The images have been labelled.

The VLA configuration was changed from A to B during our monitoring campaign. In fact, the data presented for 8.4 GHz was only for the duration of the A-array. We do not see any effects of the change of the array configuration in the light curves of the calibrators at 15GHz, giving confidence in the calibration method followed. We used the gain solutions for the phase calibrator, OQ208, to interpolate the amplitude and phase corrections for the target source.

The observations were scheduled in intervals of between 2 and 11 days. The measured flux densities are presented in Tables 1 and 2 for 8.4 and 15 GHz respectively. At 15 GHz we had 51 epochs covering both A and B configurations of the VLA. At 8.4 GHz we had only 18 epochs since its span was limited to the A configuration.

The data for B1422+231 was imaged using standard procedure in AIPS. Typical rms noise levels in the maps were about 0.3 mJy/beam at 8.4 GHz and 0.4 mJy/beam at 15 GHz. Fig. 1 shows a 15 GHz map of B1422+231 where the images have been labelled. The flux densities were measured from the maps by fitting gaussians to each of the four images using the program JMFIT. We quote the errors in flux densities as given by this program. The flux densities of the calibrators and of the four lensed images are given in Table 1 and these are plotted in Fig.2 (for 8.4 GHz results) and Table 2 and Fig. 3 (for 15 GHz results).

In what follows we chose not to analyse the results of 8.4 GHz due to insufficient points in the light curve. We concentrate on the 15 GHz results.

It is evident that any correlated variability (at the same epoch) in the light curves of calibrators as well as the target sources is due to errors in calibration. We, therefore, normalised each of the light curves of the sources by dividing it by the flux density of its first epoch. Then we divided these

Day	3C287	error	OQ208	error	A	error	B	error	C	error	D	error
0	2.1288	±0.0037	1.8110	±0.0041	0.1464	±0.0003	0.1565	±0.0003	0.0803	±0.0003	0.0041	±0.0003
1	2.1490	±0.0041	1.8104	±0.0037	0.1467	±0.0002	0.1569	±0.0002	0.0802	±0.0002	0.0040	±0.0002
11	2.1233	±0.0031	1.7412	±0.0516	0.1457	±0.0005	0.1559	±0.0005	0.0804	±0.0005	0.0045	±0.0005
15	2.1407	±0.0080	1.8119	±0.0072	0.1462	±0.0002	0.1557	±0.0002	0.0804	±0.0002	0.0043	±0.0002
18	2.1347	±0.0087	1.8069	±0.0067	0.1467	±0.0002	0.1571	±0.0002	0.0795	±0.0002	0.0045	±0.0002
21	2.1450	±0.0168	1.8175	±0.0138	0.1484	±0.0002	0.1584	±0.0002	0.0817	±0.0002	0.0044	±0.0002
25	2.1616	±0.0184	1.8463	±0.0165	0.1505	±0.0004	0.1620	±0.0004	0.0813	±0.0004	0.0036	±0.0004
28	2.1743	±0.0204	1.8335	±0.0129	0.1492	±0.0002	0.1601	±0.0002	0.0819	±0.0002	0.0045	±0.0002
31	2.1392	±0.0079	1.8070	±0.0071	0.1460	±0.0002	0.1574	±0.0002	0.0799	±0.0002	0.0040	±0.0002
36	2.1355	±0.0090	1.8066	±0.0058	0.1504	±0.0006	0.1595	±0.0006	0.0811	±0.0006	0.0047	±0.0006
38	2.1351	±0.0073	1.8020	±0.0067	0.1475	±0.0010	0.1569	±0.0010	0.0803	±0.0010	0.0042	±0.0014
40	2.1273	±0.0050	1.8211	±0.0041	0.1490	±0.0003	0.1584	±0.0003	0.0814	±0.0003	0.0043	±0.0003
46	2.1352	±0.0054	1.8197	±0.0047	0.1457	±0.0004	0.1556	±0.0004	0.0797	±0.0004	0.0042	±0.0005
51	2.1724	±0.0047	1.8260	±0.0063	0.1518	±0.0004	0.1596	±0.0004	0.0822	±0.0004	0.0042	±0.0003
53	2.0575	±0.0144	1.8130	±0.0104	0.1480	±0.0004	0.1579	±0.0004	0.0800	±0.0004	0.0039	±0.0004
58	2.1527	±0.0043	1.8227	±0.0067	0.1489	±0.0012	0.1581	±0.0012	0.0821	±0.0012	0.0069	±0.0011
63	1.9588	±0.1552	1.6580	±0.1307	0.1338	±0.0002	0.1416	±0.0002	0.0724	±0.0002	0.0040	±0.0002
68	1.9059	±0.1101	1.6057	±0.0928	0.1249	±0.0014	0.1313	±0.0014	0.0652	±0.0013	0.0038	±0.0015

Table 1. Flux densities (in Jy) of the observed sources and their errors at 8.4 GHz. The first column refers to the days starting from 1994 March 3.

normalised points by the corresponding point of OQ208 from the light curves of all the sources in order to remove the calibration errors. The rms variation in the light curve of 3C287 improved from 2.5% to 1.7% after this division (Fig. 6).

Figure 4 shows the light curves of A, B and C images of B1422+231. Figure 5 shows the light curve of image D. It is clear from Fig. 4 that we do detect variability of the three brighter images of B1422+231. Image D is rather weak and suffers from larger uncertainties due to poor signal-to-noise ratio and hence has correspondingly larger error bars. It is, therefore, not possible to conclude about its variability from the present observations. For the others, we observe peak-to-peak variability of about 5% during our observing run of 197 days.

3 NEW METHOD FOR DETERMINATION OF TIME–DELAY

In the past, the conventional method to cross-correlating the fluxes of the images to determine the time delay between them has not been very successful when the noise at the time period of expected time delay was non-negligible, even though the overall signal to noise ratio of the data could be very good. This was apparent in the case of $0957+561$ where time delay was around 417 days while some of the microlens events had similar duration (Schild & Thomson 1997, Kundić et al. 1997b, Haarsma et al. 1999). This problem is severe for B1422+231 due to the low amplitude of variability in radio.

Our method is based on identifying a single component of the intrinsic variability and using this component to cross correlate between the images (cf. Narasimha 2000). In the conventional methods, attempts are usually made to cross–correlate all the frequencies of variability simultaneously, and hence the method is most sensitive to the highest frequency. Unfortunately, the variability in the data at the highest frequency is the noise. We attempt to derive an alternative approach, in which, essentially one single frequency is analysed and the noise in the phase of this component is minimised before the feature is used for cross–correlation between the images. A smoothed cubic spline is used for the identification of the feature. We do not use any specific form for the variability, but in view of its application for many similar systems we shall illustrate and explain the general method through an ideal example where the term phase difference is easily understood.

Let the smooth component of flux obtained from the observed sample be represented by a function of the form,

$$f_\nu(t) = f_o + Asin\left[\omega\left(t-t'\right)+\phi\right]$$

Here f_o is the steady flux, A is the amplitude of variability, ω is the frequency of intrinsic variability of the signal of interest and the crucial term required for computation of the time delay is the observed phase factor ϕ for the different images.

If the external noises were absent and the sampling were sufficiently good, the flux would be

$$F_\nu(t) = F_o + \alpha sin\left[\omega_o\left(t-t'\right)+\phi_o\right]$$

We assume that α, ω_o and ϕ_o are close to the observed sample values A, ω and ϕ respectively. Then, a Taylor expansion for the sample values about the population mean is valid. Carrying out a χ^2 minimisation we can obtain four linear relations for the four unknowns. If the observations span one cycle of variability or more, the mean values for terms like $\sin(\omega t+\phi)$, $\cos(\omega t+\phi)$ summed over the observed epochs will tend to zero. Consequently, we can select a value of t' close to the mean epoch of the observation such that the computed sample values of A, ω, f_ν and ϕ will be stochastically independent. The variance of ϕ can, then, be approximated by

$$Variance(\phi) = 2/\sum_i \frac{(f_{\nu,i}-\bar{f}_\nu)^2}{\sigma_i^2}$$

Day	3C287	error	OQ208	error	A	error	B	error	C	error	D	error	Elevation
0	1.4100	±0.0064	.9243	±0.0055	0.0893	±0.0008	0.0962	±0.0008	0.0491	±0.0008	0.0024	±0.0008	76
1	1.3844	±0.0048	.9213	±0.0048	0.0886	±0.0005	0.0954	±0.0005	0.0484	±0.0005	0.0030	±0.0005	54
11	1.3879	±0.0042	.9130	±0.0039	0.0865	±0.0005	0.0931	±0.0005	0.0476	±0.0005	0.0029	±0.0006	63
15	1.3701	±0.0215	.9089	±0.0105	0.0854	±0.0006	0.0918	±0.0006	0.0474	±0.0006	0.0035	±0.0008	78
18	1.3742	±0.0101	.8953	±0.0068	0.0855	±0.0009	0.0927	±0.0009	0.0456	±0.0009	0.0030	±0.0012	78
21	1.3752	±0.0153	.9074	±0.0072	0.0861	±0.0006	0.0917	±0.0006	0.0473	±0.0006	0.0025	±0.0006	74
25	1.3501	±0.0142	.9134	±0.0038	0.0855	±0.0007	0.0938	±0.0007	0.0470	±0.0007	0.0024	±0.0005	44
28	1.4326	±0.0419	.9462	±0.0174	0.0910	±0.0007	0.0979	±0.0007	0.0487	±0.0007	0.0023	±0.0010	60
31	1.3855	±0.0142	.9069	±0.0102	0.0868	±0.0004	0.0917	±0.0004	0.0481	±0.0004	0.0022	±0.0004	79
36	1.3912	±0.0144	.9009	±0.0082	0.0877	±0.0007	0.0937	±0.0007	0.0468	±0.0007	0.0021	±0.0006	78
38	1.3784	±0.0123	.9000	±0.0106	0.0866	±0.0006	0.0934	±0.0006	0.0477	±0.0006	0.0029	±0.0007	79
40	1.3579	±0.0129	.9197	±0.0032	0.0882	±0.0005	0.0954	±0.0005	0.0475	±0.0005	0.0031	±0.0005	57
46	1.3871	±0.0045	.9227	±0.0043	0.0884	±0.0007	0.0930	±0.0007	0.0482	±0.0007	0.0034	±0.0008	56
51	1.4061	±0.0061	.9329	±0.0083	0.0904	±0.0007	0.0978	±0.0007	0.0502	±0.0007	0.0017	±0.0006	76
53	1.3507	±0.0210	.9270	±0.0097	0.0904	±0.0008	0.0976	±0.0008	0.0502	±0.0009	0.0014	±0.0006	76
58	1.4131	±0.0055	.9374	±0.0083	0.0905	±0.0007	0.0977	±0.0007	0.0504	±0.0007	0.0030	±0.0008	77
63	1.3799	±0.0095	.9456	±0.0063	0.0917	±0.0006	0.0974	±0.0006	0.0489	±0.0006	0.0028	±0.0007	66
68	1.4028	±0.0053	.9011	±0.0040	0.0891	±0.0007	0.0960	±0.0007	0.0478	±0.0007	0.0028	±0.0007	74
70	1.3892	±0.0066	.9109	±0.0046	0.0884	±0.0009	0.0981	±0.0010	0.0509	±0.0010	0.0047	±0.0012	63
74	1.4092	±0.0034	.9193	±0.0029	0.0909	±0.0006	0.0966	±0.0006	0.0498	±0.0006	0.0015	±0.0006	76
79	1.4194	±0.0064	.9453	±0.0040	0.0922	±0.0006	0.0988	±0.0006	0.0501	±0.0007	0.0028	±0.0008	72
85	1.3948	±0.0070	.9136	±0.0050	0.0901	±0.0007	0.0976	±0.0008	0.0480	±0.0008	0.0026	±0.0009	74
89	1.4072	±0.0091	.9086	±0.0088	0.0902	±0.0007	0.0968	±0.0007	0.0491	±0.0007	0.0029	±0.0008	76
95	1.3673	±0.0035	.9179	±0.0038	0.0904	±0.0006	0.0983	±0.0006	0.0497	±0.0006	0.0028	±0.0006	44
100	1.3676	±0.0082	.9158	±0.0033	0.0928	±0.0006	0.1000	±0.0006	0.0497	±0.0006	0.0023	±0.0006	44
104	1.3731	±0.0037	.9205	±0.0028	0.0895	±0.0007	0.1007	±0.0007	0.0505	±0.0007	0.0022	±0.0007	44
108	1.3480	±0.0057	.9174	±0.0032	0.0913	±0.0007	0.0997	±0.0007	0.0500	±0.0007	0.0033	±0.0010	44
112	1.4018	±0.0064	.9109	±0.0032	0.0896	±0.0008	0.0974	±0.0008	0.0482	±0.0008	0.0020	±0.0007	74
115	1.3663	±0.0052	.9220	±0.0031	0.0908	±0.0007	0.0992	±0.0007	0.0505	±0.0007	0.0033	±0.0008	44
119	1.3938	±0.0053	.9147	±0.0043	0.0912	±0.0007	0.0973	±0.0007	0.0494	±0.0007	0.0025	±0.0006	78
122	1.3714	±0.0114	.9280	±0.0088	0.0928	±0.0007	0.0994	±0.0007	0.0506	±0.0007	0.0025	±0.0007	44
130	1.3726	±0.0035	.9236	±0.0025	0.0915	±0.0006	0.1039	±0.0007	0.0500	±0.0006	0.0031	±0.0007	38
133	1.3966	±0.0032	.9144	±0.0027	0.0905	±0.0004	0.0976	±0.0004	0.0494	±0.0005	0.0031	±0.0006	69
140	1.3464	±0.0131	.9212	±0.0039	0.0909	±0.0006	0.0975	±0.0006	0.0496	±0.0006	0.0021	±0.0006	63
147	1.3991	±0.0116	.9131	±0.0043	0.0900	±0.0007	0.0982	±0.0007	0.0493	±0.0007	0.0026	±0.0007	57
154	1.4964	±0.0472	.9133	±0.0076	0.0997	±0.0008	0.1067	±0.0008	0.0531	±0.0008	0.0033	±0.0009	72
159	1.3155	±0.0098	.9257	±0.0036	0.0849	±0.0007	0.0918	±0.0007	0.0463	±0.0008	0.0023	±0.0007	79
168	1.5046	±0.0224	.9933	±0.0216	0.0941	±0.0009	0.1005	±0.0009	0.0512	±0.0006	0.0028	±0.0006	79
173	1.4648	±0.0209	.8518	±0.0087	0.0927	±0.0008	0.0982	±0.0008	0.0460	±0.0017	0.0025	±0.0009	74
175	1.4148	±0.0051	.9458	±0.0068	0.0917	±0.0007	0.0984	±0.0007	0.0509	±0.0010	0.0024	±0.0006	78
186	1.3729	±0.0083	.8128	±0.0274	0.0904	±0.0006	0.0984	±0.0007	0.0493	±0.0008	0.0019	±0.0007	44
189	1.3928	±0.0047	.9776	±0.0102	0.0895	±0.0006	0.0953	±0.0006	0.0498	±0.0007	0.0030	±0.0006	68
192	1.3564	±0.0057	.9497	±0.0104	0.0903	±0.0007	0.0985	±0.0007	0.0489	±0.0006	0.0033	±0.0007	44
197	1.3875	±0.0094	.9269	±0.0031	0.0863	±0.0007	0.0925	±0.0007	0.0488	±0.0006	0.0000	±0.0000	29

Table 2. Flux densities (in Jy) of the observed sources and their errors at 15 GHz. The first column refers to the days starting from 1994 March 3. The last column gives the elevation of B1422+231 in degrees. The flux densities of the two calibrators, 3C287 and OQ208 were determined from the program GETJY while that of lensed images were determined by fitting a gaussian to the image.

The time-delay between the images can be estimated from the cross-correlation between the variable part of the fluxes obtained from the smoothed cubic splines. The cross correlation will have the form

$$R = cos\left(\omega\tau + \phi_1 - \phi_2\right),$$

where τ is the assumed time delay between the images. The phase factors ϕ_1 and ϕ_2 refer to the variable components of the smoothed cubic spline fits to the observed fluxes in the images 1 and 2. The errors in the data points are contributed almost entirely by the calibration source and the steady part of the signal. The time period over which the source is monitored is very long compared to the time–delay. Consequently, the variance in R can be approximated, to a good extent, by the product of the variance of the normalised flux of the two images. As we described earlier, since we are interested only in the phase factor of the variable component of the fluxes, the errors in the normalised smoothed flux represent the errors in the computed phase factor. The variance is an indicator of the expected error in the computed flux and hence, the estimated time–delays. If the smoothed flux has exactly the same form in the images, the correlation will have a peak value of unity, but in practice it will be less when the fitting is done independently. In view of the form of the expression for R, the error in the computed time delay is the time interval over which the correlation, R, drops by

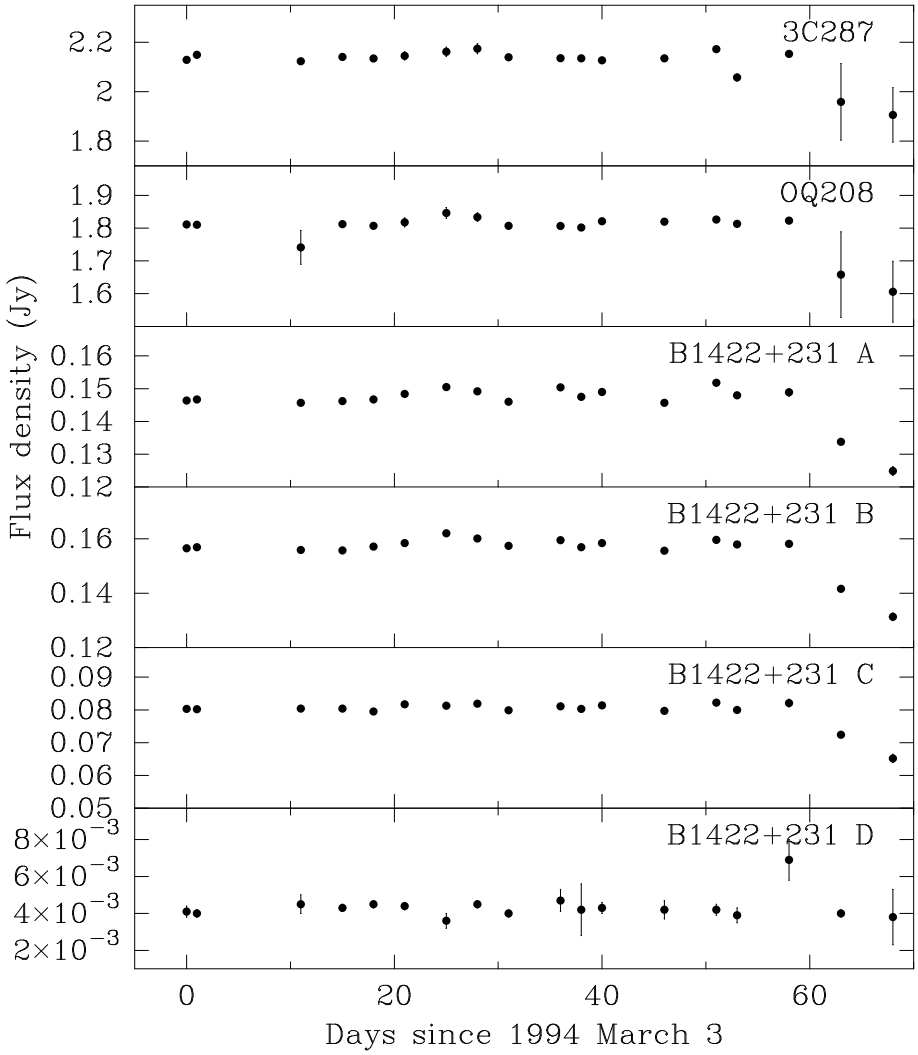

Figure 2. Light curves for the observed sources at 8.4 GHz. Source name is indicated in the respective panel.

half the estimated variance of the phase ϕ of the smoothed fit to the flux.

4 RESULTS

For the system B1422+231, the 15 GHz observations were spread over 197 days and a variability of 5.2% was detected. We estimate the period of variability to be about 216 days. The observations were carried out at intervals of 2 to 11 days. It is reasonable to assume that the observations lasted for one cycle of variation. For the 8.4 GHz, the observations lasted for less than seventy days, number of epochs were less. Consequently, we are not able to carry out the analysis discussed here. Hence our time–delay analysis is restricted to the 15 GHz data.

The variances of ϕ for the images B, A and C are at 0.013 level which is equivalent to 4 days (variance of 0.01 is equivalent to an error of 0.1 radian, and as the period is about 216 days, this amounts to about 4 days). This is a consequence of the time interval between the observations being at 2 to 11 days. Since the time intervals between observations are not fixed, we are able to separate a time–delay of less than the minimum time interval between the successive observations. But our computed error is rather high which shows that with a better sampling of the observations we should be able to get time–delays for all the images. In practice, the uncertainty in the relative fluxes of the images is mainly due to the day to day calibration error rather than the relative flux of the images with respect to the calibrator. Hence, strictly, the stochastic independence of the data cannot be claimed. Nevertheless, we treat the normalised fluxes of images to be stochastically independent. This results in higher error estimate.

However, for the image D, the error in individual observations is considerable due to the faintness of the image. Consequently, the estimated variance of the phase is around 7, corresponding to an uncertainty of over 150 degrees, implying that the relative phase of image D with respect to other images cannot be estimated from the given sample. So, we have not carried out any analysis for this image, in spite of its significance for cosmological purposes. The derived

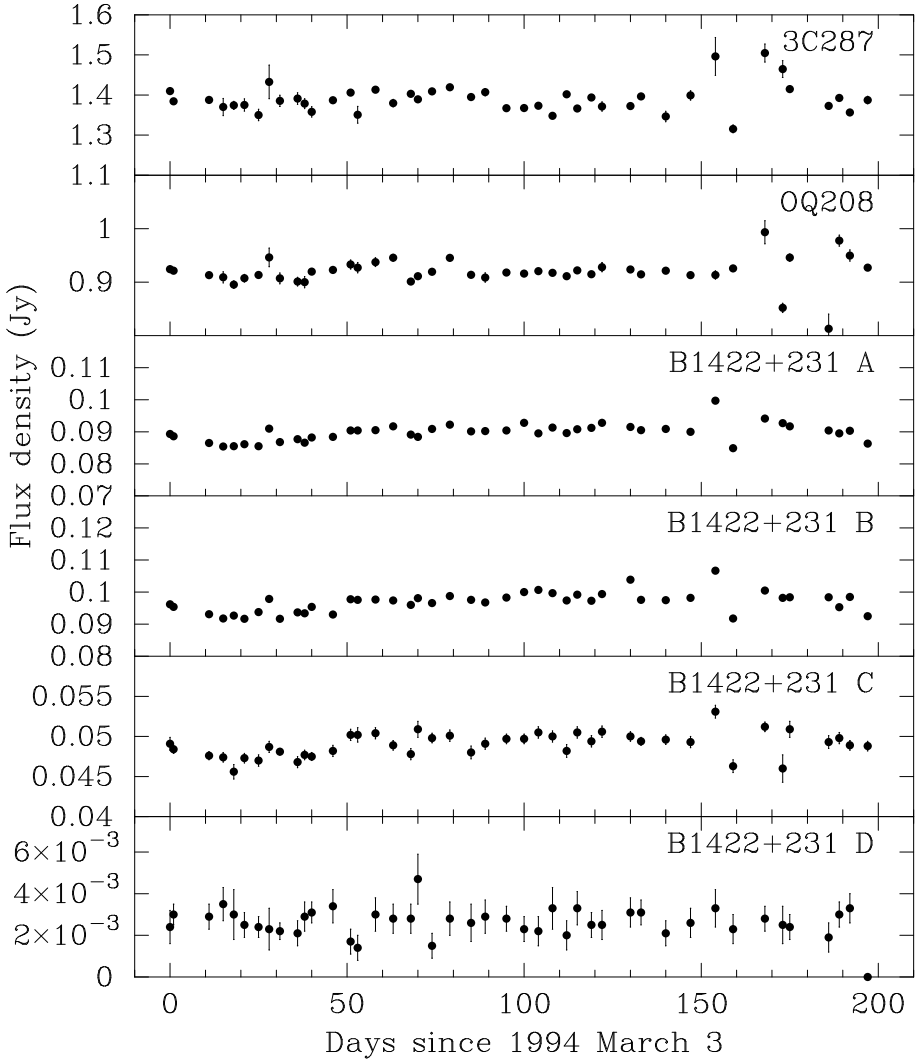

Figure 3. Light curves of the observed sources at 15 GHz. Source name is indicated at the respective panel.

time delays between images B and A is 1.5±1.4d, between A and C is 7.6±2.5d and between B and C is 8.2±2.0d.

When is this method superior to direct estimation of the time delay? If the smoothed cubic spline can isolate a single component of the intrinsic flux variability from the mean flux of the images, and any contribution due to microlensing is filtered from the smooth function, then the signal in the correlation will improve compared to the noise by a factor of (n-4), where n is the number of epochs of observation and the number 4 is based on the minimum number of data points required for the computations of the smoothed spline. In practice, the errors between the various images are not independent because as in the case of our data for B1422+231, the main contribution to error in the smoothed fit is from the calibrating sources which are common to all the images. Consequently, our error estimate is probably conservative; the time delays could be closer to our estimations than the error bars suggest. This can be seen also from the fact that the sum of the time delays between images BA and between AC agrees well with that of BC.

5 DISCUSSION

The time delays between the images A, B and C have been determined, though not very accurately. However, the monitoring of the weaker image D has not been successful mainly because the fractional errors in the flux densities were considerably larger than the amplitude of the intrinsic variability. For the distance estimate, the time delay between image D and other images is important because it is a measure of the lens mass. Hence our results, so far, do not provide any reliable distance determination. It would be necessary to carry out monitoring for a longer time with considerably better precision in order to estimate the time delay between image D and the brighter images.

The models of Narasimha & Patnaik (1993) predicted a value of time delay between images A and C of the order of 9 days for a distance to the lens of 1000 Mpc (signal appearing in C first), assuming a single component lens and H_0 to be 50 km s $^{-1}$Mpc^{-1}. Our measurement of AC time delay of 7.6±2.5d implies a Hubble constant in the range of 64 to 75 km s^{-1} Mpc^{-1} for the standard cosmology, with only a

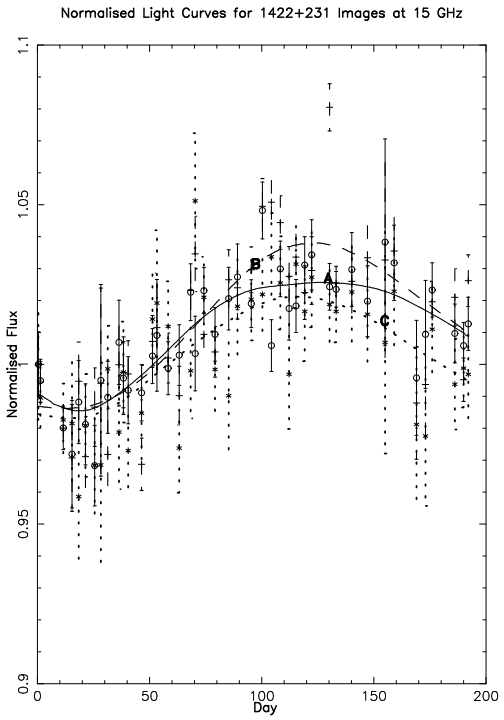

Figure 4. Smoothed light curves (spline fit) of images A (∘), B (+) and C (⋆) of B1422+231 at 15 GHz. The light curves have been normalised. Observations for individual epochs are marked with 1σ error bars. The X-axis refers to the days since 1994 March 3.

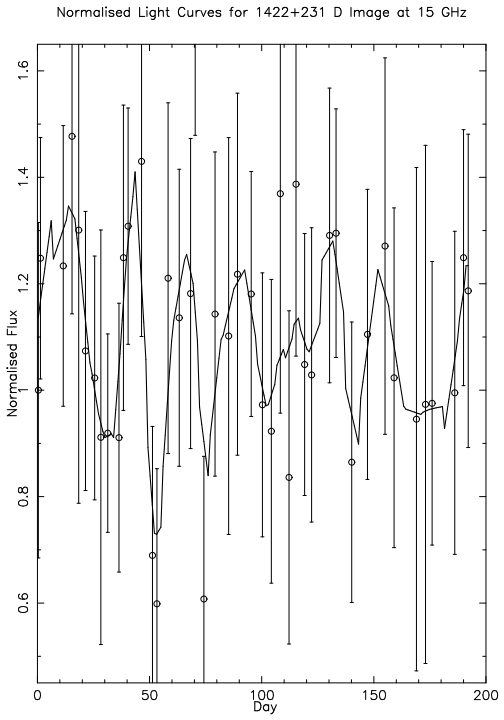

Figure 5. Normalised light curve of image D of B1422+231 at 15 GHz. The X-axis refers to the days since 1994 March 3. The solid line is the spline fit.

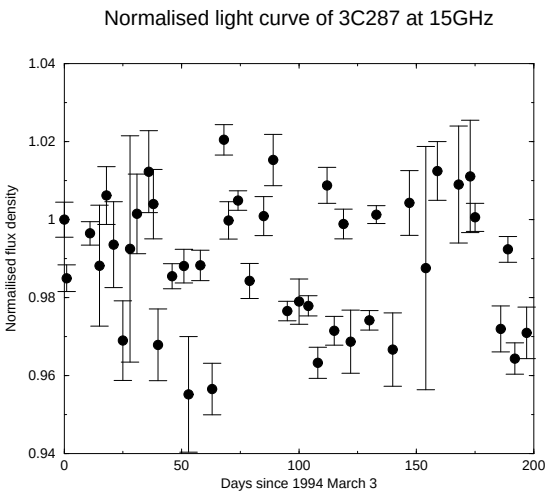

Figure 6. Normalised light curve of the calibrator 3C287 after dividing it by that of OQ208. No systematic variability is observed in this light curve.

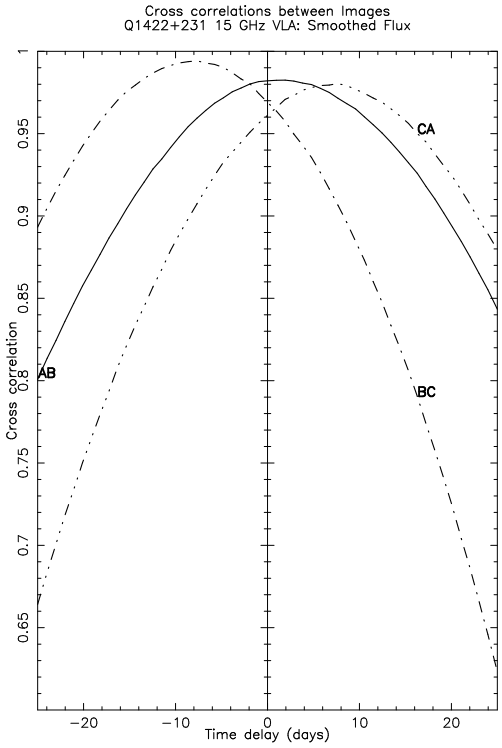

Figure 7. Cross correlation between the images of B1422+231 at 15 GHz using the smoothed light curve as explained in the text.

weak dependence on Ω and Λ. Narasimha & Srianand (1999) considered abstract models comparing the caustic structure near the images A, B and C using the flux ratios in the emission lines, optical and radio continuum. Their result cannot be directly translated into time delay, but if the size of Lyman emission region is less than 10^{17} cm, a large scale length of the lens is implied and the Hubble constant turns out to be less than 35 km s^{-1} Mpc^{-1}. Since there is evidence for

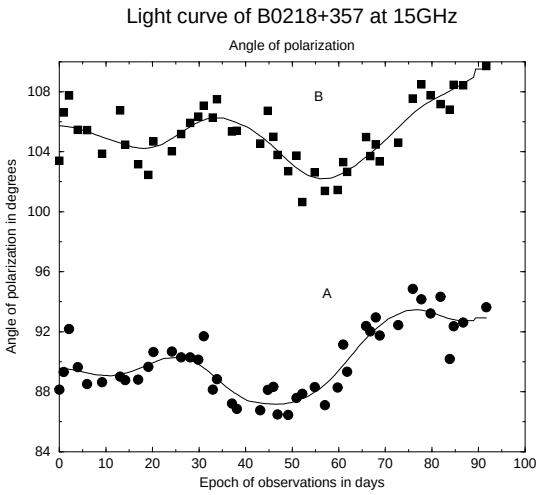

Figure 8. Smoothed curve (spline fit) through the observed data (position angle of polarization) of B0218+357 at 15GHz. Light curves for images A and B are labelled. Data are taken from Biggs et al. (1999).

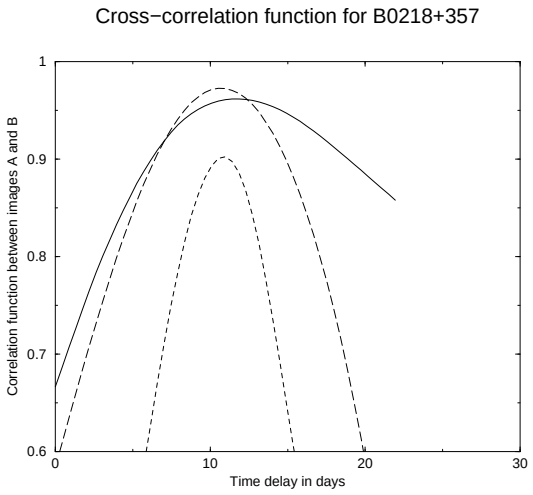

Figure 9. Cross-correlation function for the light curve of B0218+357. Solid line represents the correlation function for the total intensity, long dashed curve represents that for the position angle of polarization, and small dashed curve represents that for the fractional polarization of B0218+357 at 15GHz. Data are taken from Biggs et al. (1999).

a weak group of galaxies near the main lens, the result is expected to be in between the two limits discussed above.

However, a natural question to address is that whether the method suggested here is reliable and has advantages over the conventional data analysis techniques. We shall briefly address these questions by showing our results and some comments for the three systems, namely, B1608+656, B0218+357 and PG1115+080, for which time delays have been available during the last few years, but the data are still not good compared to 0957+561.

6 VARIABILITY AND TIME–DELAY IN OTHER LENS SYSTEMS

We have analysed the available data for the systems B1608+656 (Fassnacht et al., 1999), B0218+357 (Biggs et al., 1999) and PG1115+080 (Schechter et al., 1997). We have displayed one typical diagram for the time delay based on polarization angles in the system B0218+357 (Fig. 8) and a summary of the results for the three systems is given in Table 3.

The data for B1608+656 are very good, in spite of low amplitude of the variability and multi-component fluctuations. The excellent calibration based on stable reference source and elimination of the questionable data make the derived time delay reliable. Our results for the three combination of the time delays (AB, BC and BD) are in good agreement with the value derived by the observers' team, and the value for AB is very close to the differential time delay BC-AC. However, it would be worth pointing out that the smoothed spline cross–correlation peaks at much lower than 1, which indicates that there could be considerable amount of noise introduced en route in all the images. Possibly multi-frequency observations and polarization data would be required to assess the nature of this noise.

For the system B0218+357, at the higher frequency, all the three methods, namely, total flux, polarization fraction and the the polarization angle give nearly identical results (Fig. 9 and Table 3), all in agreement with the values given by the observers' team. The polarization angle appears to have the highest correlation between the images in our method. We think that polarization angle is among the most trustworthy indicators of the intrinsic variability, as pointed out by Nair et al. (1993) and Nair (1994).

For the system PG1115+080, again, our results are broadly in agreement with Schechter et al. (1997). However, a few comments are worth mentioning. First, the time delay between images B and C are generally stable against analysis technique or some amount of noise in the data. But the time–delay between the merging image A and the other two are sensitive to the method adopted as well as the noise in the reference star. Second, for the whole data, our time–delay between images B and C is slightly smaller than the value given by Schechter et al. But if we drop two days on which the fluctuation in the magnitude of the reference star was comparable to the amplitude of variability of the quasar, the time–delay becomes 24.4 days, which is exactly in between the values derived by Schechter et al. and Barkana (1997). Third, our value for the time delay between images A and B range from 6 to 11 days, depending on using or dropping the data for the two days. The corresponding value for the time–delay between images C and A vary between 14 and 13 days. Consequently, our time–delay ratio between CA and AB are always consistent with the lens models; the small ratio supports a compact lens and higher value for the Hubble constant while the larger ratio favours an extended lens and smaller Hubble constant.

Table 3. *Comparison of time–delay analysis for three lens systems:*

The method developed here is used for the recent data available for three lenses and the results are compared.

System	Images	Observers Time-delay (days)	Present Technique Time-delay (days)	Reference
B1608+656	Δt_{BA}	31±7	30.4±4.5	Fassnacht et al. (1999)
	Δt_{BC}	36±7	37.6±4.5	
	Δt_{BD}	76^{+9}_{-10}	75.3±4.2	
	Δt_{AC}		4.5±4.5	
B0218+357				Biggs et al. (1999)
15 GHz:				
Flux	Δt_{AB}	$10.6^{+0.7}_{-0.5}$	11.6±2	
Polarization fraction		11.4±0.3	11.4±1	
Polarization angle		$10.2^{+0.3}_{-0.4}$	11.2±2	
8.4 GHz:				
Flux		$10.1^{+1.4}_{-0.7}$	‡	
Polarization fraction			14.4±3	
Polarization angle			8.4±3	
PG1115+080	Δt_{CB}	23.7±3.4	19.6±5.4	Schechter et al.(1997)
	Δt_{CA}	9.4±3.4	12.4±4.8	
	Δt_{AB}	14.3±3.4	6.7±4.8	
*	Δt_{CB}		24.4±4.8	
	Δt_{CA}		13.6±4.2	
	Δt_{AB}		10.3±4.2	

* After eliminating two days when the reference star exhibited considerable fluctuation.
‡ The smoothed cubic spline did not converge and hence we cannot get a time–delay for the total flux.

7 CONCLUSIONS

We have monitored B1422+231 with the VLA at two different frequencies. The light curves were sampled at intervals of 2 to 10 days only because we did not have a good idea of the amplitude of intrinsic variability and were interested in the image D in view of its importance for cosmological distance calibration. Consequently, we are unable to get very accurate value for the time delay between images. But we are able to determine the time delay between the bright images using the 15 GHz observations, obtaining 1.5, 7.6 and 8.2 days for AB, CA and CB time delays respectively. More extensive monitoring at significantly higher signal to noise ratio is necessary to determine the time delay between the weak image D and the other images.

ACKNOWLEDGMENTS

We would like to thank J. Schmid-Burgk and K.M. Menten for critical comments and the comments of an anonymous referee which resulted in improving the presentation of the paper. We have made use of information available at the CASTLE web-site (http://cfa-www.harvard.edu/glensdata/) for gravitational lenses maintained by C.S. Kochanek, E.E. Falco, C. Impey, J. Lehár, B. McLeod and H.-W. Rix. We are grateful to NRAO for their support in carrying out these observations. The National Radio Astronomy Observatory is a facility of the National Science Foundation operated under cooperative agreement by Associated Universities, Inc. DN acknowledges support from Indo-French Centre for the promotion of Advanced Research, through contract 1410-2.

REFERENCES

Akujor, C.E., Patnaik, A.R., Smoker, J.V., Garrington, S.T., 1996, in Kochanek, C.S, Hewitt, J.N., eds, Proceedings of the 173rd Symposium of the IAU 'Astrophysical applications of gravitational lensing', Kluwer Academic Publishers, Dordrecht, p335
Barkana, R., 1997, ApJ, 489, 21
Bechtold, J., Yee, H.K.C., 1995, AJ, 110, 1984
Biggs, A.D., Browne, I.W.A., Helbig, P., Koopmans, L.V.E., Wilkinson, P.N., Perley, R.A., 1999, MNRAS, 304, 349
Fassnacht, C.D., Pearson, T.J., Readhead, A.C.S., Browne, I.W.A., Koopmans, L.V.E., Myers, S.T., Wilkinson, P.N., 1999, ApJ, 527, 498
Haarsma, D.B., Hewitt, J.N., Lehár, J., Burke, B.F., 1999, ApJ, 510, 64
Hogg, D.W., Blandford, R.D., 1994, MNRAS, 268, 889
Impey, C.D., Foltz, C.B., Petry, C.E., Browne, I.W.A., Patnaik, A.R., 1996, ApJ, 462, L53
Koopmans, L.V.E., de Bruyn, A.G., Xanthopolous, E., Fassnacht, C.D., 2000, AA, in press
Kormann, R., Schneider, P., Bartlemann, M., 1994, A&A, 286, 357
Kundić, T., Hogg, D.W., Blandford, R.D., Cohen, J.G., Lubin, L.M., Larkin, J.E., 1997a, AJ, 114, 2276
Kundić, T., Turner, E.L., Colley, W.N., Gott, III,R., Rhoads , J.E., Wang, Y., Bergeron, L.E., Gloria, K.A., Long, D.C., Malhotra, S., Wambsganss, J., 1997b, ApJ, 482, 75

Lawrence, C.R., Neugebauer, G., Weir, N., Matthews, K., Patnaik, A.R., 1992, MNRAS, 259, 5P
Lovell, J., Jauncey, D.L., Reynolds, J.E., Wieringa, M.H., King, E.A., Tzioumis, A.K., McCulloch, P.M., Edwards, P.G., 1998, ApJ, 508, L51
Mao, S., Schneider, P., 1998, MNRAS, 295, 587
Nair, S., 1994, Ph.D. Thesis, Bombay University, unpublished
Nair, S. Narasimha, D., Rao, A.P., 1993, ApJ, 407, 46
Narasimha, D., 1999, Pramana, 53, 921
Narasimha, D., 2000, in Rencontres de Moriond, Les Arcs, eds. Y. Mellier, J.-P. Kneib & M. Moniez
Narasimha, D., Patnaik, A.R., 1994, in Surdej, J., Fraipont-Caro, D, Grosset, E., Refsdal, S., Remy, M., eds, Proc. 31st Liège International Astrophysical Colloq., Gravitational Lenses in the Universe, Université de Liège, Belgique, p.295
Narasimha, D., Srianand, R., 1999, in Bulletin of Astronomical Society of India (in press)
Patnaik, A.R., Browne, I.W.A., Walsh, D., Chaffee, F.H., Foltz, C.B., 1992, MNRAS, 259, 1P
Patnaik, A.R., Kemball, A.J., Porcas, R.W., Garrett, M.A., 1999, MNRAS, 307, L1
Refsdal, S., 1964, MNRAS, 128, 307
Remy, M., Surdej, J., Smette, A., Claeskens, J.-F., 1993, AA, 278, L19
Schild, R., Thomson, D.J., 1997, AJ, 113, 130
Schechter, P.L., Bailyn, C. D., Barr, R., Barvainis, R., Becker, C. M., Bernstein, G. M., Blakeslee, J. P., Bus, Schelte J., Dressler, A., Falco, E. E., Fesen, R. A., Fischer, P., Gebhardt, K., Harmer, D., Hewitt, J. N., Hjorth, J., Hurt, T., Jaunsen, A. O., Mateo, M., Mehlert, D., Richstone, D. O., Sparke, L. S., Thorstensen, J. R., Tonry, J. L., Wegner, G., Willmarth, D. W., Worthey, G., 1997, ApJ, 475, 85
Tonry, J.L., 1998, AJ, 115, 1
Yee, H.K.C., Bechtold. J., 1996, AJ, 111, 1007
Yee, H.K.C., Ellingson, E., 1994, AJ, 107, 28

This paper has been produced using the Royal Astronomical Society/Blackwell Science LaTeX style file.